RESEARCH PAPER

The Effect of Powder Composition on the Cyclic Oxidation Behavior of Co-Deposited Al-Si Coating on Nickel-Base Superalloy

M. Ghasemian Safaei, S. Rastegari* and R. Latifi

**rastegari@iust.ac.ir*

Received: March 2019 Revised: September 2019 Accepted: January 2020

* School of Metallurgy and Materials Engineering, Iran University of Science and Technology, Tehran, Iran.

DOI: 10.22068/ijmse.17.2.104

Abstract: *In this study, Si-modified aluminide coating on nickel-base superalloy IN-738LC was prepared using a pack cementation method with various powder compositions at 1050 °C for 6 h. The cyclic oxidation test was conducted at 1000 °C followed by cooling at room temperature for 200 h and 20 cycles. The effect of powder composition and the way of cooling on the coatings microstructure and oxidation behavior were studied. Investigations carried out using a scanning electron microscope (SEM), EDS analysis, and XRD. Microstructural observations revealed that the coating thickness of 293 and 274 µm was achieved in the case of using pure Al and Si powder and alloyed Al-20wt.%Si one in the packed mixture, respectively. It was also found that utilizing pure Al and Si powder with NH4Cl as an activator in the pack led to the formation of silicide coating, owing to the higher diffusion of Si, which showed superior cyclic oxidation performance.*

Keywords: *Si-modified aluminide coating, Cyclic oxidation, Pack cementation, Superalloys.*

1. INTRODUCTION

Diffusion aluminide coatings are primarily used in aerial applications to protect the substrate which is mainly Ni and/or Co-based superalloy against oxidative environment at high temperature. However, aluminide coating composed of β-NiAl is brittle and susceptible to sulfur segregation in grain boundaries, leading to the substrate interface weakening and oxide spallation [1–3]. To substantially increase their performance particularly the oxidation and corrosion resistance in a hostile environment, sufficient quantities of elements such as Pt, Si, Hf, and Zr can be added into the aluminide coating either separately or simultaneously [4–8]. It has been reported that the modification of aluminide diffusion coatings by silicon has noticeably improved its oxidation and corrosion resistance [9–11]. Zhou and coworkers [12] fabricated Al-Si coatings on Ti–6Al–4V alloy by means of the low oxygen pressure fusing technology. They indicated that oxidation-resistant elements Al and Si in the coating played a major role in enhancing the oxidation resistance of the Ti–6Al–4V alloy. Kim and Jung [13] produced Si-containing aluminide coating on low carbon steel by varying the SiO_2 content in the pack as the source of Si. It was found that good oxidation properties were achieved with Si concentration of approximately 3 wt.% at the surface of the coating. Xiang et al. [14] investigated the feasibility of co-depositing Al and Si to form a multiple-element diffusion coating on Ni-based superalloy using pack cementation.

Nevertheless, detailed studies on the microstructure of co-deposited Al-Si coating acquired from different powder compositions in the pack before and after cyclic oxidation have been very limited. Thus, attempts have been made to examine the influence of different parameters on the microstructures and oxidation behavior of the modified aluminide coating, i.e. Al and Si sources, activators, and the way of cooling samples.

2. EXPERIMENTAL

IN-738LC is used as the substrate in this research and coatings applied using the pack

cementation method. The powder mixture contained NH_4Cl or $AlCl_3$ activators, pure Al and Si or alloyed Al-20Si as a metallic source, and alumina as the filler. The sample size was 10×10×3 mm and their surfaces were grounded using 80, up to 1200 SiC sandpapers before coating. Then, they were washed with acetone, dried, and placed in the neutral alumina retort filled with the powder mixture. The alumina retort and lid were sealed using chamotte, kaolin, and sodium silicate glue, and all were put into the resistance furnace. The furnace heated up to 1050 °C, remained at this temperature for 6 h, and then turned off. The samples were cooled in the furnace to reach the room temperature apart from one sample which was cooled out of the furnace. Additionally, the cyclic oxidation tests were conducted in static air to determine the oxidation resistance of the coating. Each cycle consisted of 10 h in a furnace at 1000 °C followed by 30 minutes cooling down to room temperature. Cyclic oxidation behavior was investigated after 20 cycles of heating and cooling. The mass change was measured after each cycle. To easily describe the coating conditions, a coding system was used at which A20S and A-S represent the use of alloying source, pure Al, and pure Si in the chemical composition of the coating powder, respectively. Also, the letters N and A after the mentioned symbols represent the use of NH_4Cl and $AlCl_3$ activators, respectively. Finally, the letters I and O at the end of the codes represent the cooling method after the cyclic oxidation, which expresses the cooling in the furnace and out of the furnace, respectively. Table 1 shows coating conditions for the samples. Microstructures of the coated samples before and after cyclic oxidation were studied by scanning electron microscope (SEM) equipped with Energy Dispersive Spectroscopy (EDS) analyzer. In addition, the phase composition of the coatings after cyclic oxidation was investigated using the X-Ray Diffractometer (XRD).

3. RESULTS AND DISCUSSION

3.1. Effect of Pure and Alloyed Sources with NH_4Cl Activator

The cross-sectional SEM images of the Si-modified aluminide coatings (A20SN-I and A-SN-I samples) with different Al and Si sources in the pack powder after their co-deposition by the pack cementation process are shown in Fig. 1. While Al-20wt.%Si alloyed powder was used for the A20SN-I sample, the A-SN-I sample was prepared using the pure Al and Si powders as metallic sources. As mentioned in the experimental section, the activator component and its quantity, as well as Al content, were the same for both A20SN-I and A-SN-I samples. The coating microstructure of the A20SN-I specimen is similar to the typical aluminide coating, whereas the A-SN-I coating has a silicide microstructure. Both coatings comprised an outer layer and a small interdiffusion zone underneath. Considering the EDS analysis results (Table. 2 and 3), the outer layer of the A20SN-I coating contained evenly distributed small precipitates with a high concentration of Cr, Co, and Ti, whereas these elements are soluble in the outer layer of A-SN-I coating. As it can be observed, the A-SN-I coating has a higher thickness of 293 μm in comparison to the A20SN-I coating with a thickness of 274 μm. This can be possibly due to more activity of the elements in the case of being pure compared

Table 1. Coating conditions of samples.

Coating Symbol	Al (Wt. %)	Si (Wt. %)	Al-20Si (Wt.%)	$AlCl_3$ (Wt. %)	NH_4Cl (Wt. %)	Al_2O_3 (Wt. %)	Cooling after coating formation
A20SN-I	---	---	2.875	---	4	93.125	In the furnace
A-SN-I	2.3	15	---	---	4	78.7	In the furnace
A-SN-O	2.3	15	---	---	4	78.7	Out of the furnace
A20SA-I	---	---	2.875	3.327	---	93.798	In the furnace
A-SA-I	2.3	15	---	3.327	---	79.373	In the furnace

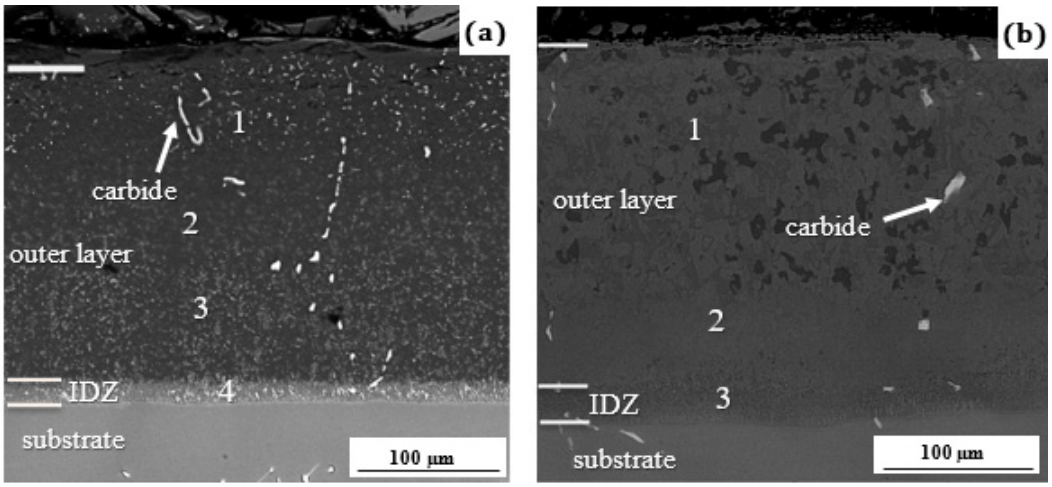

Fig. 1. Cross-sectional SEM image of the Si-modified aluminide coatings obtained by NH_4Cl activator and (a) Al-20Si (wt.%) source (A20SN-I sample) (b) pure sources of Al and Si (A-SN-I sample)

with alloyed nature in the pack powder mixture, leading more diffusion capability in the coating. Furthermore, the Si content in pack mixture has a higher amount of 15 wt.% when the pure metallic source of Si was used compared with the alloyed source of Si with 0.575 wt.% which resulted in generating a higher Si-halide vapor pressure and more diffusion of Al and Si in the substrate.

Based on the EDS result (Table. 2), there is a high amount of Al with low content of Si within the coating of the A20SN-I sample. As the quantities of elements in the powder were directly related to their activities, a higher quantity of an element in the packed powder provided a higher activity ending up in a higher halide vapor pressure and diffusion. Therefore, Al activity was more than that of Si, leading to produce higher Al-halide vapor pressure and more diffusion in the coating. However, in the case of A-SN-I coating, the Si concentration within the outer coating layer and the interdiffusion zone is relatively high, whereas the Al content is low, which is owing to the large amount of Si source in the packed mixture and as a result, the activator could transport and deposit more Si on the substrate.

3. 2. Effect of Pure and Alloyed Sources with $AlCl_3$ Activator

The microstructure of the A20SA-I and A-SA-I coatings are presented in Fig. 2a and b, respectively. Both coatings microstructures

Table 2. EDS analysis of the A20SN-I coating points marked in Fig. 1a (at. %).

point	Ni	Al	Si	Cr	Ti	Co
1	16	70.4	0.7	4.1	1.2	1.8
2	26.5	65.8	1.1	2.6	0	1.8
3	24.3	64.9	2.7	3.7	0.1	3
4	32.5	27.3	0	23.9	5.9	5.5

Table 3. EDS analysis of the A-SN-I coating points marked in Fig. 1b (at. %).

point	Ni	Al	Si	Cr	Ti	Co
1	46.5	0.1	37.5	6.9	1	5.9
2	30.8	0.01	39.3	14.8	3.2	6
3	28.1	9.1	26.7	18.9	3.9	5.8

are similar to the aluminide coating with small precipitates containing a high concentration of refractory elements of Co, Cr, and Ti in the outer layer. Compared with the A20SA-I sample with a thickness of 118 µm, the A-SA-I sample has more thickness of 159 µm, which is in accordance with the reported results in the prior section. Based on the coatings EDS analysis in Tables 4 and 5, when $AlCl_3$ was used as an activator, the amount of Si was lower than the Al percentage for both coatings. Particularly, within the A-SA-I sample, despite the higher percentage of Si as the primary source in the powder mixture, the composition of the vapor phase formed in the pack was more favorable for depositing Al. The reason is that $AlCl_3$ is more intended to activate Al as compared with Si, which led to the generation of more Al halide vapor pressure and then more Al diffusion [14]. For the A20SA-I sample, Si percentage was very low and almost the same in all layers of coating for it was low in the powder source and did not have any considerable diffusion into the coating. Similarly, according to the Table 5 which is related to the A-SA-I sample, a lower amount of Si exists in the surface and near the inter-diffusion zone compared with the middle of the coating since initially, $AlCl_3$ cannot react with Si creating a high Si-halide vapor pressure, and as a result, Al vapor pressure went on the rise. Over the passage of time, by reducing of Al in the primary source and thereby decreasing its vapor pressure, Si has become capable of diffusing along with Al. Finally, with a small amount of Si in the primary source, its activity, vapor pressure, and diffusion were reduced.

3.3. Effect of Different Activators with Alloyed Source

According to Figs. 1a and 2a, the coating microstructure of the Si-modified aluminide coating with alloyed source and various activa-

Table 4. EDS analysis of the A20SA-I coating points marked in Fig. 2a (at. %).

point	Ni	Al	Si	Cr	Ti	Co
1	28.8	63	0.6	3.5	0	3.4
2	30.1	59.2	0	5.5	0.6	4.2
3	30.5	28.9	0.8	24.5	5.7	5.1

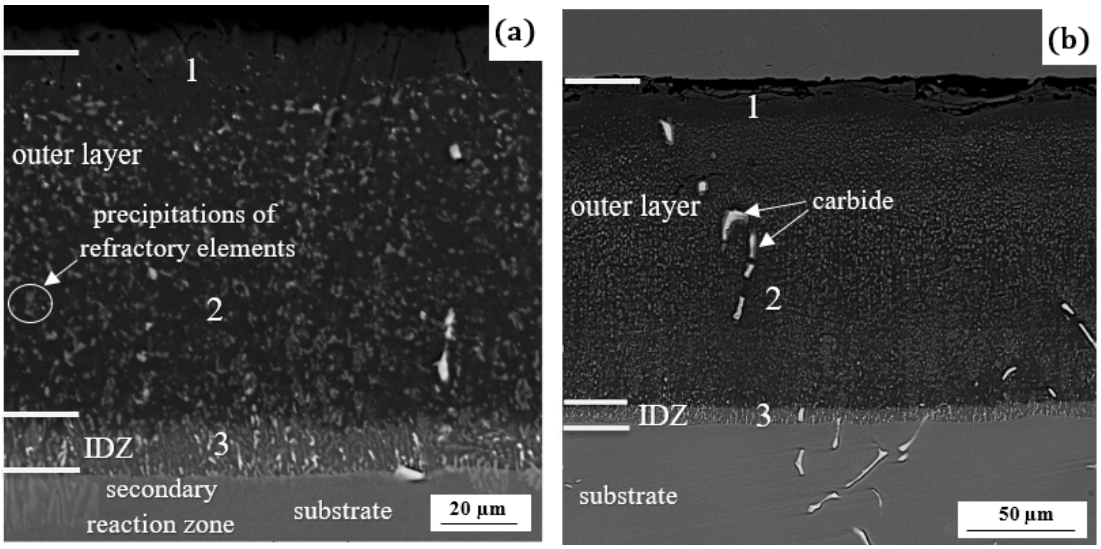

Fig. 2. Cross-sectional SEM image of the Si-modified aluminide coatings obtained by $AlCl_3$ activator and (a) Al-20Si (wt.%) source (A20SA-I sample) (b) pure sources of Al and Si (A-SA-I sample)

Table 5. EDS analysis of the A-SA-I coating points marked in Fig. 2b (at. %).

point	Ni	Al	Si	Cr	Ti	Co
1	37.2	53.2	3.1	0.6	0.2	3.6
2	30.6	44.5	10.7	7.1	1.3	3.8
3	30.6	17	5.8	25.2	8.1	5

tors (A20SN-I and A20SA-I samples) are similar to that of the simple aluminide coating. The composition of both coatings is a mixture of Al and Ni with tiny precipitations of refractory elements. Based on the EDS analysis which its results are summarized in Tables 2 and 4, the inter-diffusion zone was mainly composed of Ti and Cr. The coating thickness obtained for the A20SN-I sample (274 µm) was more than the A20SA-I one (118 µm) due to the low stability of the NH_4Cl activator compared with $AlCl_3$ [11]. Accordingly, NH_4Cl could react more easily with Al and Si contained in the pack powder mixture and increase the produced halide vapor pressures, resulting in more depositing of Al and Si on the substrate and their diffusion into the coating. In fact, the vapor pressures of species produced by various activators are different because of their disparate tendencies to perform reactions and in this regard, NH_4Cl had more tendency to react with Al and Si [15]. Besides, the amount of Al was higher than Si in both coatings because only 20% of the alloy was made of Si and the remaining 80% was composed of Al. Therefore, Si activity was very low leading to its slight diffusion.

3.4. Effect of Different Activators with Pure Source

The same result is achieved in the case of using pure source and various activators so that the coating thickness of the A-SN-I sample is higher than that of the A-SA-I sample. For the A-SN-I sample, Si percentage was very high while Al content was extremely low; the reason lies in the fact that the amount of Si was much more than Al in the powder mixture of this sample. While the Si weight percentage in the pack was the same for both A-SN-I and A-SA-I samples, more Si content can be observed within the

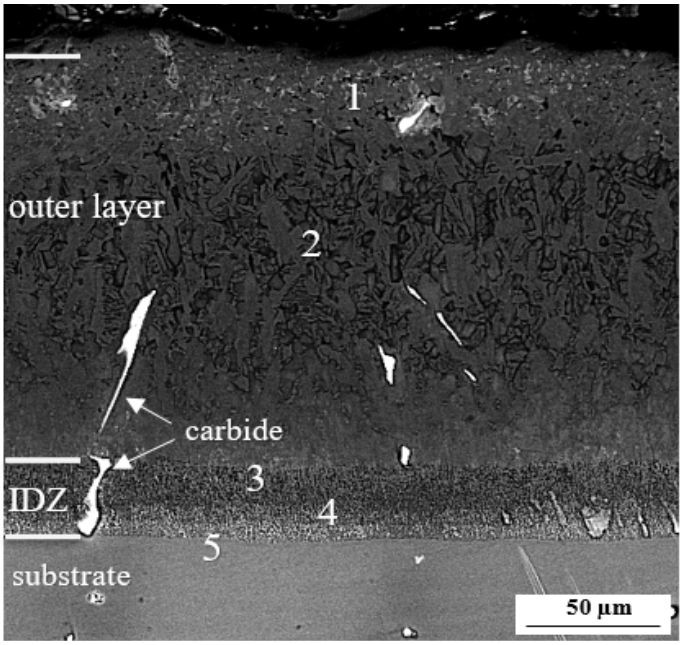

Fig. 3. Cross-sectional SEM image of the Si-modified aluminide coatings obtained by Al and Si source of pure and NH4Cl activator, then cooled out of the furnace (A-SN-O sample).

Table 6. EDS analysis of the A-SA-O coating points marked in Fig. 3 (at. %).

point	Ni	Al	Si	Cr	Ti	Co
1	34.7	1	30.5	0.6	0.2	3.6
2	50.8	1.3	28.2	7.1	1.3	3.8
3	29.6	6.6	22.2	25.1	8.1	5

outer coating layer of A-SN-I specimen, which confirms that NH4Cl as an activator had more capability in generating sufficiently high Si-halide vapor pressure. Regarding the high content of Si and Ni within the outer coating layer of A-SN-I sample, it could be assumed that the outer layer has consisted of Ni_2Si phase rich in Si [16], and the remaining Si would be soluble in this phase or has formed a new phase with chromium [17].

3.5. Effect of Cooling Method on Microstructure

Fig. 3 illustrates the cross-sectional microstructure of the Si-modified aluminide coating which was aluminized with NH_4Cl activator and then cooled out of the furnace (A-SN-O coating). Based on Fig. 3 and EDS analysis in Table 6, the coating exhibits the same silicide microstructural features as the A-SN-I coating. The A-SN-O sample has a coating thickness of 170 µm which is less than that of A-SN-I sample (293 µm) due to the cooling out of the furnace resulted in being less time at high temperature. It is known that time is one of the diffusion parameters and diffusion influences the thickness.

3.6. Microstructures and Compositions of Oxidized Coatings

As indicated in Fig. 4, the weight changes curve of the samples exhibited an intense weight increase due to the formation of an oxide layer during early moments. The results of the A20SA-I sample have been rejected because of the severe degradation after the first cycle. The sharp weight loss observed in the A20SN-I sample after only 2 cycles demonstrated the poor resistance to cyclic oxidation at 1000 °C. The mass change curve of the A-SA-I and the A-SN-O coatings consisted of three regions; oxide formation (0-30h), steady-state oxidation (30-130h), and oxide spallation (after 130h). As the XRD patterns are shown (Fig. 5), the presence of Cr_2O_3 and NiO phases besides Al_2O_3 and SiO_2 in an oxide scale resulted in poor oxidation resistance.

In contrast, the A-SN-I sample does not have a significant change in weight, which indicates

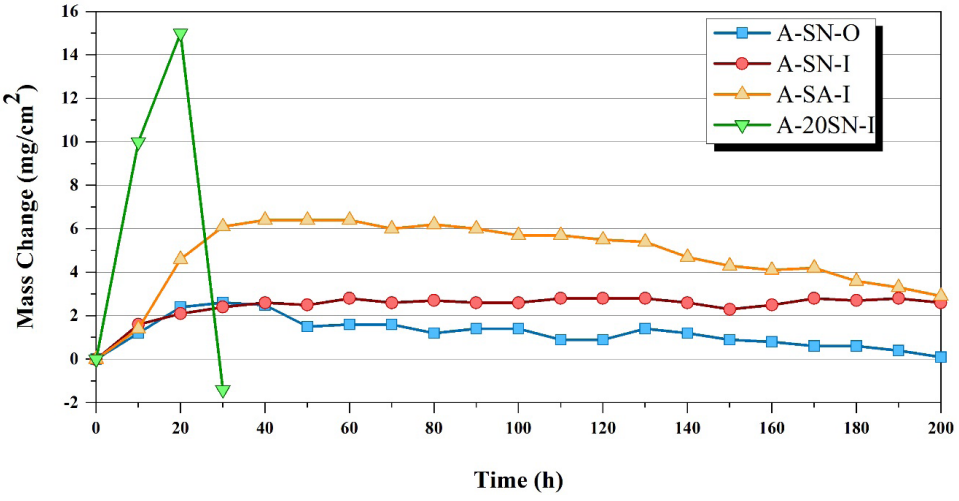

Fig. 4. Weight change during 200 h cyclic oxidation at 1000 °C.

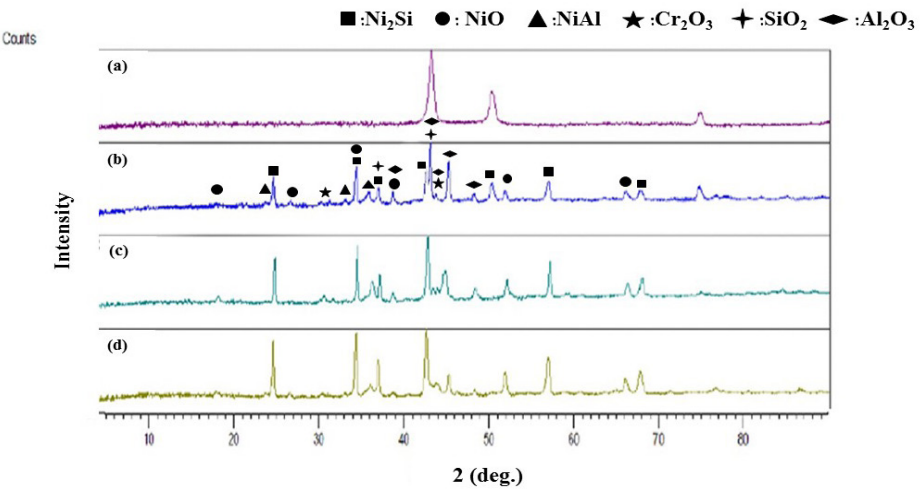

Fig. 5. X-ray diffraction patterns for the substrate and the Si modified aluminide coatings after 200 h cyclic oxidation at 1000 °C (a) substrate without any coating before oxidation (b)A-SN-O coating, (c) A-SA-I coating and d) A-SN-I sample.

good protection of the oxide layer. Since the coating contains higher concentrations of Al and Si on the surface that form more stable oxide scales in the cyclic oxidizing environment as indicated in EDS analysis (Table 3). Also, a notable amount of silicon oxide in the oxide scale can probably result in decreasing of oxygen uptake because of its glassy phase [16]. In comparison to the A-SA-I and the A-SN-O coatings, there are few Cr_2O_3 and NiO phases in the case of A-SN-I sample, which reveals that higher silicon content delays the formation of harmful phases of Cr_2O_3 and NiO.

3.7. Effect of Cooling Conditions

As shown in Fig. 6, there are light gray zones (A) in the matrix of the oxidized A-SN-O sample which contain Ni, Si, and dissolved Ti elements (Table 7). These zones have extensively existed all over the coating before the oxidation process, they were though decreased after the oxidation test, due to the formation of NiAl [18]. The EDS results show that Si is enriched near the inter-diffusion zone which represents the inward diffusion of Si [16]. While the surface microstructure of the A-SN-O coating after 200 h of cyclic oxidation at 1000 °C demonstrates the formation of aluminum oxide (Table 7), a small amount of Ni and Cr are present in the mentioned region, indicating the existence of Cr_2O_3 and NiO along with Al_2O_3 (Fig. 5). This proves that the oxide scale spallation has occurred, resulting in Al outward diffusion to the surface to repair the oxide layer and inward diffusion of the oxygen into the coating through the spalled regions. According to the Ellingham diagram, owing to more stability of Al_2O_3, selective oxidation will occur in those regions. In fact, if there exists enough Si oxide, the inward diffusion of oxygen does not occur through the oxide scale [17]. The chemical composition analysis of point 2, presented in Table 7, detected the Al and Ni with a concentration of 20 at.% and 56 at.%, respectively as well as

Table 7. EDS analysis of A-SN-O sample after 200 h cyclic oxidation at 1000 °C (at. %).

point/zone	Co	Ti	Cr	Si	Al	Ni	O
1	0.07	0	0.09	0.52	40.66	0.46	55.51
2	5.9	1.35	7.95	4.06	20.42	56.04	0.81
3	6.81	3.47	17.68	10.42	10.29	39.41	6.51
A	5.39	11.72	2.43	28.39	0.1	49.53	0.5

extremely low amount of oxygen, indicating the prevention of oxygen diffusion into the interior layer of the coating.

Beneath the inter-diffusion zone, some needle-like precipitates, known as TCP, are observed which are formed due to the outward diffusion of Ni from the substrate. These precipitates are one of the reasons for the occurrence of sudden spallation of the coating [19] which led to the inward diffusion of the oxygen into the substrate.

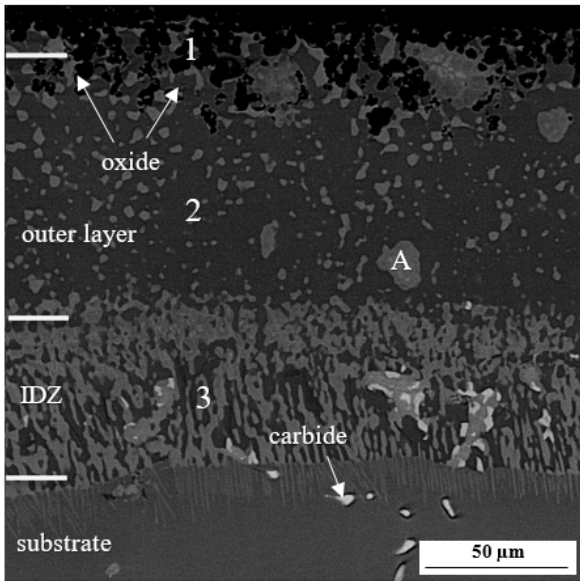

Fig. 6. Cross-sectional SEM image of A-SN-O sample after 200 h cyclic oxidation at 1000 °C.

The SEM micrograph and EDS analysis of the oxidized A-SN-I sample after 200 h of cyclic oxidation and cooling in the furnace, show that the coating surface (point 1) generally consists of aluminum oxide (Fig. 7 and Table 8). Indeed, as there was a high concentration of Si within the coating, selective oxidation of aluminum has occurred. Moreover, there was a small amount of Cr in this region which is due to the presence of chromium oxide (as seen in Fig. 5). Compared with the oxidized A-SN-O sample which was cooled out of the furnace, there is no inward diffusion of oxygen, which can be attributed to the higher content of Si within the coating, leading to the production and outward diffusion of aluminum and prevention of inward diffusion of oxygen. Furthermore, oxygen atoms have less ability to diffuse through the Si oxide [20]. Hence, it can be concluded that, by increasing the Si concentration prior to the oxidation, Si oxide hinders the inward diffusion of oxygen which improves the oxide scale adhesion to the coating and enhances the oxidation resistance. As can be observed, there are a small amount of Al and more Si within the oxidized A-SN-I coating. It is because of the presence of a higher concentration of Si in the coating before the oxidation process. However, the concentration of Si is reduced compared to before oxidation, which is attributed to the Si consumption during the oxidation and the formation of [Al] [16]. Moreover, the presence of Ti and Cr in the form of precipitates in addition to Si in the inter-diffusion zone show the silicide of refractory elements formation [21].

Consequently, in comparison to the oxidized A-SN-O sample, lack of the NiO and low content of the Cr_2O_3 along with the Al_2O_3 demonstrate the good protection of the oxide scale and superiority of the A-SN-I sample during the oxidation condition.

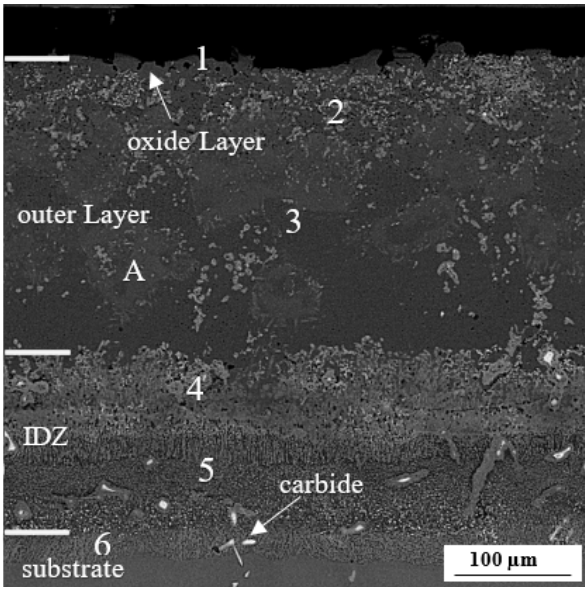

Fig. 7. Cross-sectional SEM image of A-SN-I sample after 200 h cyclic oxidation at 1000 °C.

3.8. Effect of Different Activator

As can be seen in Fig. 8, the surface of the oxidized A-SA-I sample is mainly composed of aluminum oxide (Table 9). Prior to the oxidation, the coating contained a high concentration

Table 8. EDS analysis of A-SN-I sample after 200 h cyclic oxidation at 1000 °C (at. %).

Layer/zone	Co	Ti	Cr	Si	Al	Ni	O
1	0.3	0.1	2.1	1.5	32.1	0.9	56.2
2	4.6	0.4	14.7	30.1	0.1	42.4	2.4
3	7.3	4.4	6.6	32.7	1.1	43.5	0.1
4	6.3	3.4	11.8	30.6	1.3	42.1	0.2
5	4.9	4.1	22.4	21.7	8.4	27.9	3.4
6	7.2	3.9	23.6	12.8	10.9	35.8	0.1
A	8.2	7.1	5.7	35.8	0.7	39.3	1.7

Table 9. EDS analysis of A-SA-I sample after 200 h cyclic oxidation at 1000 °C (at. %).

point	Co	Ti	Cr	Si	Al	Ni	O
1	0.3	0.1	2.1	1.5	44.5	0.9	44.8
2	5.6	0.7	7.1	9.7	27.3	46.7	0.4
3	4.8	0.8	5.3	32.7	30.5	48.6	0.1
4	6.3	5.2	15.3	13.8	13.7	37.9	0.1
5	8	3.7	23.1	6.8	12.4	36.3	2.6
6	6.5	4.7	19.7	3.7	10.6	46.8	0.1

of aluminum and a small amount of Si. Hence, lack of sufficient Si within the coating caused a low content of aluminum oxide on the coating surface, meaning that most of which was pulled off from the surface and resulted in severe oxide spallation and weight loss (as shown in Fig. 4). According to the EDS analysis (Table 9) that is in agreement with the XRD result (Fig. 5c), Ni and Cr oxide were formed within the oxide scale which confirms the lack of oxide layer protection during the oxidation condition and as a result, the substrate was oxidized.

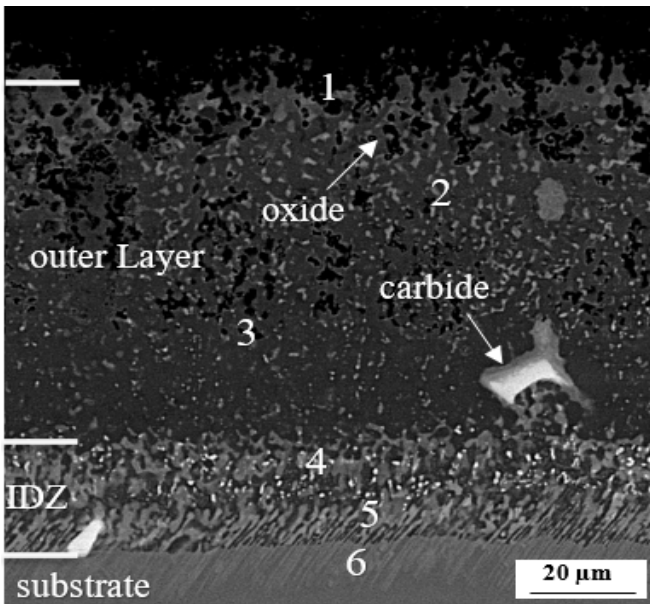

Fig. 8. Cross-sectional SEM image of A-SA-I sample after 200 h cyclic oxidation at 1000 °C.

3.9. Effect of Al and Si in Powder Source

Based on the SEM cross-section image of the oxidized A20SN-I sample (Fig. 9) and EDS analysis (Table 10), there is a higher level of aluminum within the coating compared with other samples because this sample was removed from the oxidation test due to the severe weight loss since the 14th cycle. So, as a result of incomplete cycles of oxidation, little aluminum content has consumed. Further, there is much Ti and Cr oxide along with some Ni oxide in the surface which shows the diffusion of these elements to the surface and oxide scale spallation. The reason is attributed to the lack of silicon oxide near aluminum oxide to enhances the oxide scale adhesion and inhibit the formation of detrimental oxides. Accordingly, the protection of this coating is not sufficient in the oxidation condition which is consistent with the result of the weight change curve (Fig. 4).

4. CONCLUSIONS

1. In the case of pure source of Al and Si, coating thickness with the same activator and aluminum content was higher than the thickness obtained for the sample aluminized with an alloyed source of Al and Si.
2. The coating thickness of the sample aluminized using NH_4Cl as an activator was more than that of one prepared by $AlCl_3$ as an activator.
3. Increasing Si content in the coating caused an improvement in the cyclic oxidation resistance. Indeed, Si not only prevents the formation of non-protective NiO oxide which forms due to the failure of the Al_2O_3 but also increases the stability range of Al_2O_3 and improves the adhesion of the oxide layer.
4. The oxidation resistance of the coatings is better when pure Al and Si is used as the

Table 10. EDS analysis of A20SN-I sample after 200 h cyclic oxidation at 1000°C (at. %).

point	Co	Ti	Cr	Si	Al	Ni	O
1	0.2	1.5	4.4	1.3	33.9	0.6	56.5
2	5	0.8	11.8	0.8	34.1	36.6	8
3	5.1	1.8	20	2.7	27.8	31.7	5.7
4	5.6	1.8	6.2	0.3	33.6	48	0.1
5	4.8	4.0	24.2	2.1	20.5	34.5	3.8
6	9.2	4.9	26.2	1.7	14.4	35.5	0.1

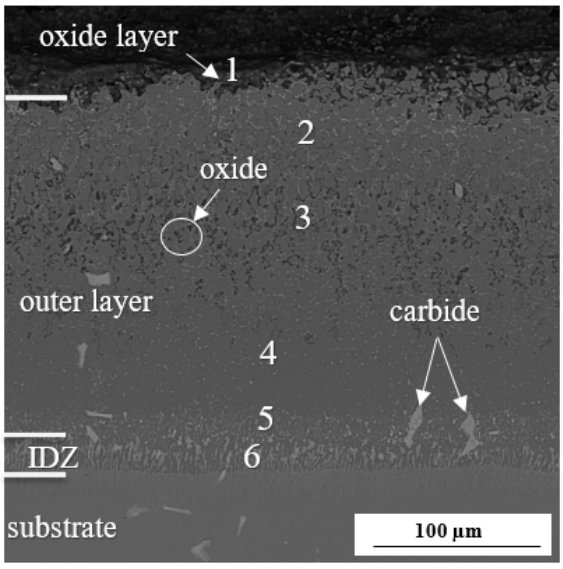

Fig. 9. Cross-sectional SEM image of A20SN-I sample after 200 h cyclic oxidation at 1000°C.

initial source in comparison to the alloyed source or activated by NH4Cl compared with AlCl3.

REFERENCES

1. Deodeshmukh, V. and Gleeson, B., "Evaluation of the hot corrosion resistance of commercial β-NiAl and developmental γ′-Ni3Al + γ-Ni-based coatings", Surf. Coatings Technol. 202, 2007, 643–647. doi:10.1016/j.surfcoat.2007.06.018.
2. Rafiee, H., Rastegari, S., Arabi, H., Mojaddami, M., "Effects of temperature and al-concentration on formation mechanism of an aluminide coating applied on super alloy in738lc through a single-step high activity gas diffusion process", Iran. J. Mater. Sci. Eng. 7, 2010, 42–49.
3. Nouri, S., Rastegari, S., Mirdamadi, S., Hadavi, M., "Formation of Diffusion Aluminide Coatings on γ-TiAl Alloy with In-Pack and Out-Pack Processes", Trans. Indian Inst. Met. 68, 2015, 867–871. doi:10.1007/s12666-015-0523-y.
4. Wang, J., Kong, L., Wu, J., T. Li, T. Xiong, Microstructure evolution and oxidation resistance of silicon-aluminizing coating on γ-TiAl alloy, Appl. Surf. Sci. 356, 2015, 827–836. doi:10.1016/j.apsusc.2015.08.204.
5. Liu, R. D., Jiang, S. M., Yu, H. J., Gong, J., Sun, C., "Preparation and hot corrosion behaviour of Pt modified AlSiY coating on a Ni-based superalloy", Corros. Sci. 104, 2016, 162–172. doi:10.1016/j.corsci.2015.12.007.
6. Das, D. K., "Microstructure and high temperature oxidation behavior of Pt-modified aluminide bond coats on Ni-base superalloys", Prog. Mater. Sci. 58, 2013, 151–182. doi:10.1016/j.pmatsci.2012.08.002.
7. Li, D., Guo, H., Peng, H., Gong, S. and Xu, H., "Improved alumina scale adhesion of electron beam physical vapor deposited Dy/Hf-doped β-NiAl coatings", Appl. Surf. Sci. 283, 2013, 513–520. doi:10.1016/j.apsusc.2013.06.137.
8. Latifi, R., Rastegari, S. and Razavi, S. H., "Effect of Zr Content on Oxide-scale Spallation of Aluminide Coating", Iran. J. Mater. Sci. Eng. 16, 2019, 63–72. doi:10.22068/ijmse.16.4.63.
9. Shirvani, K., Saremi, M., Nishikata, A. and Tsuru, T., "The effect of silicon on cyclic oxidation behavior of aluminide coatings on superalloy IN-738LC", Mater. Sci. Forum. 461–464, 2004, 335–342. doi:10.4028/www.scientific.net/msf.461-464.335.
10. Wang, Q. M., Wu, Y. N., Ke, P. L., Cao, H. T., Gong, J., Sun, C. and Wen, L. S., "Hot corrosion behavior of AIP NiCoCrAlY(SiB) coatings on nickel base superalloys", Surf. Coatings Technol. 186, 2004, 389–397. doi:10.1016/j.surfcoat. 2003.12.020.
11. Jiang, S. M., Peng, X., Bao, Z. B., Liu, S. C., Wang, Q. M., Gong, J. and Sun, C., "Preparation and hot corrosion behaviour of a MCrAlY + AlSiY composite coating", Corros. Sci. 50, 2008, 3213–3220. doi:10.1016/j.corsci.2008.08.018.
12. Zhou, W., Zhao, Y. G., Li, W., Qin, Q. D., Tian, B. and Hu, S. W., "Al-Si coating fused by Al + Si powders formed on Ti-6Al-4V alloy and its oxidation resistance", Mater. Sci. Eng. A. 430, 2006, 142–150. doi:10.1016/j.msea.2006.05.115.
13. Kim, M. T. and Jung, J. S.,"Codeposition of Al and Si onto a low carbon steel using silicon dioxide and aluminum and its hot temperature oxidation properties", Surf. Coatings Technol. 161, 2002, 218–223. doi:10.1016/S0257-8972(02)00498-X.
14. Xiang, Z. D. and Datta, P. K., "Codeposition of Al and Si on nickel base superalloys by pack cementation process", Mater. Sci. Eng. A. 356, 2003, 136–144. doi:10.1016/S0921-5093(03)00107-2.
15. Wang, L., Pan, L. L., Peng, H., Guo, H. B. and Gong, S. K.,"Cyclic oxidation behavior of Cr-/Si-modified NiAlHf coatings on single-crystal superalloy produced by EB-PVD", Rare Met. 35, 2016, 396–400. doi:10.1007/s12598-015-0482-9.
16. Fu, C., Kong, W. K. and Cao, G. H., "Microstructure and oxidation behavior of Al+Si co-deposited coatings on nickel-based superalloys", Surf. Coatings Technol. 258, 2014, 347–352. doi:10.1016/j.surfcoat.2014.09.003.
17. Van Roode, M. and Hsu, L., "Evaluation of the hot corrosion protection of coatings for turbine hot section components", Surf. Coatings Technol. 37, 1989, 461–481. doi:10.1016/0257-8972(89)90084-4.
18. Sivakumar, R. and Mordike, B. L., "High tem-

perature coatings for gas turbine blades: A review", Surf. Coat. Technol. 37, 1989, 139–160. doi:10.1016/0257-8972(89)90099-6.
19. Angenete, J., Stiller, K., Bakchinova, E., "Microstructural and microchemical development of simple and Pt-modified aluminide diffusion coatings during long term oxidation at 1050 °C", Surf. Coatings Technol. 176, 2004, 272–283. doi:10.1016/S0257- 8972(03)00767-9.
20. Firouzi, A. and Shirvani, K., "The structure and high temperature corrosion performance of medium-thickness aluminide coatings on nickel-based superalloy GTD-111", Corros. Sci. 52, 2010, 3579–3585. doi:10.1016/j.corsci.2010.06.026.
21. Azarmehr, S. A., Shirvani, K., Schütze, M. and Galetz, M., "Microstructural evolution of silicon-platinum modified aluminide coatings on superalloy GTD-111", Surf. Coatings Technol. 321, 2017, 455–463. doi:10.1016/j.surfcoat.2017.05.019.